frontiers | Frontiers in Nanotechnology

TYPE Brief Research Report
PUBLISHED 20 November 2023
DOI 10.3389/fnano.2023.1267284

OPEN ACCESS

EDITED BY
Hamed Barabadi,
Shahid Beheshti University of Medical Sciences, Iran

REVIEWED BY
Linhan Lin,
Tsinghua University, China
Mubarak A. Mujawar,
Florida International University, United States
Tianqing Jia,
East China Normal University, China

*CORRESPONDENCE
Koji Sugioka,
ksugioka@riken.jp

RECEIVED 26 July 2023
ACCEPTED 31 October 2023
PUBLISHED 20 November 2023

CITATION
Kawabata S, Bai S, Obata K, Ozasa K, Miyaji G and Sugioka K (2023), Formation of two-dimensional laser-induced periodic surface structures on titanium by GHz burst mode femtosecond laser pulses.
Front. Nanotechnol. 5:1267284.
doi: 10.3389/fnano.2023.1267284

Formation of two-dimensional laser-induced periodic surface structures on titanium by GHz burst mode femtosecond laser pulses

Shota Kawabata[1,2], Shi Bai[1], Kotaro Obata[1], Kazunari Ozasa[1], Godai Miyaji[2] and Koji Sugioka[1]*

[1]Advanced Laser Processing Research Team, RIKEN Center for Advanced Photonics, Wako, Japan, [2]Department of Applied Physics, Tokyo University of Agriculture and Technology, Koganei, Japan

GHz burst mode femtosecond (fs) laser pulses, which consist of a series of pulse trains with ultra-fast intervals of several hundred picoseconds, have offered distinct features for material processing compared to conventional irradiation of laser pulses (single-pulse mode). We apply GHz burst mode processing to fabricate laser-induced periodic surface structures (LIPSS) on the material surfaces. In our previous work for silicon (Si), we have found that GHz burst mode can create unique two-dimensional (2D) LIPSS composed of both parallel and perpendicular to the laser polarization direction. We proposed that the formation of 2D-LIPSS is attributed to the synergetic contributions of electromagnetic and hydrodynamic mechanisms. To further investigate more detailed formation mechanisms and explore practical applications, we employ titanium (Ti), whose properties are significantly different from Si. We demonstrate that GHz burst mode fs laser pulses (central wavelength: 1,030 nm, intra-pulse width: 230 fs, intra-pulse repetition rate (an intra-pulse interval): 4.88 GHz (205 ps) and burst pulse repetition rate: 10 kHz) can also fabricate 2D-LIPSS on Ti surfaces. We attribute the dominant formation mechanism of 2D-LIPSS to the generation of hot spots with highly enhanced electric fields due to transient change of material properties during GHz burst pulse irradiation. Based on this speculation, properly tailoring the shapes of the burst pulse with an optimum intra-pulse number enables the creation of well-defined 2D-LIPSS. Furthermore, essentially homogeneous 2D-LIPSS can be formed in a large area by laser scanning of a focused fs laser beam with a stage scanning speed of 5 mm/s.

KEYWORDS

femtosecond laser pulse, GHz burst mode, laser-induced periodic surface structures (LIPSS), surface nanostructuring, 2D-periodic nanostructures, lattice-like structures

1 Introduction

It is well known that femtosecond (fs) laser pulses with linear polarization can form laser-induced periodic surface structures (LIPSS) exhibiting stripe-like patterns on the surfaces of various solid materials. These materials can include metals (Tsukamoto et al., 2006; Vorobyev and Guoa, 2008; Okamuro et al., 2010; Bonse et al., 2012; Oya et al., 2012; Nathala et al., 2015; Shinonaga et al., 2015; Shinonaga et al., 2016; Tamamura and Miyaji,

2019), semiconductors (Borowiec and Haugen, 2003; Wagner et al., 2007; Huang et al., 2009; Bonse and Krüger, 2010; Miyaji et al., 2012; Miyazaki and Miyaji, 2013; Tjy et al., 2014; Kawabata et al., 2023), polymers (Wagner et al., 2007; Sato et al., 2016) and dielectric substances (Shimotsuma et al., 2003; Wagner et al., 2007; Edakubo et al., 2022). The characteristics of LIPSS, including size, shape and orientation, are highly dependent on the laser wavelength (Borowiec and Haugen, 2003; Wagner et al., 2007; Nathala et al., 2015; Bai et al., 2023), pulse width (Nathala et al., 2015; Shinonaga et al., 2016; Bai et al., 2023) and fluence (that is, the pulse energy) (Shimotsuma et al., 2003; Okamuro et al., 2010; Bonse et al., 2012; Miyaji et al., 2012; Nathala et al., 2015) as well as the number of laser pulses applied (Shimotsuma et al., 2003; Tsukamoto et al., 2006; Huang et al., 2009; Bonse and Krüger, 2010; Bonse et al., 2012; Miyaji et al., 2012; Miyazaki and Miyaji, 2013; Nathala et al., 2015; Shinonaga et al., 2016), the polarization direction (Varlamova et al., 2006; Reif et al., 2008; Bai et al., 2023) and the irradiation environment (Miyaji et al., 2012; Tjy et al., 2014). Typically, the period of LIPSS fabricated using a fs laser will be smaller than the laser wavelength, indicating the potential for laser surface nanostructuring beyond the diffraction limit. On this basis, LIPSS are expected to have a number of applications, such as the reduction of friction (Bonse et al., 2014) and the control of optical properties (Vorobyev and Guoa, 2008; Tamamura and Miyaji, 2019; Edakubo et al., 2022) as well as surface-enhanced Raman spectroscopy (Bai et al., 2018; Bai et al., 2020; Bai et al., 2023) and the control of cell growth (Oya et al., 2012; Shinonaga et al., 2015; Sato et al., 2016; Shinonaga et al., 2016). Consequently, the development of simple, contact-free laser irradiation technologies not requiring complex environments would be beneficial with regard to industrial applications. Several mechanisms intended to explain the formation and characteristics of LIPSS have been proposed to date, including the generation of nanoplasmas (Buividas et al., 2011) and second harmonics (Borowiec and Haugen, 2003; Dufft et al., 2009) together with self-organization based on instabilities resulting from symmetry breaking at the surface (Varlamova et al., 2006), surface temperature modulation (Gurevich, 2016; Levy et al., 2016) and the excitation of surface plasmon polaritons (SPPs) (Bonse and Krüger, 2010; Miyaji et al., 2012; Miyazaki and Miyaji, 2013; Tjy et al., 2014; Iida et al., 2021). To date, however, a consensus has not been reached.

Recently, our group discovered that linearly polarized, burst mode fs laser pulses applied at frequencies in the GHz range can create distinctive two-dimensional (2D) LIPSS on single-crystalline Si surfaces (Kawabata et al., 2023). These periodic surface structures were found to form either perpendicular or parallel to the direction of laser polarization. The formation of 2D-LIPSS in this manner can likely be attributed to a synergetic combination of electromagnetic and hydrodynamic effects. Specifically, it appears that a one-dimensional (1D) LIPSS are initially fabricated by preceding intra-pulses in the GHz burst pulse, and at the same time, the silicon surface simultaneously becomes metal-like due to electron excitation. Consequently, hot spots associated with highly enhanced electric fields induced by localized surface plasmon resonance (LSPR) are periodically generated at the sidewalls of nanogrooves in the 1D-LIPSS by subsequent intra-pulses. These hot spots ablate the sidewalls of the structure but, because they do not, etch the entire width of the ridges, these ridges are narrowed. The sidewalls at which hot spots are not generated are melted based on a small increase in the electric field. Following this, opposing melted regions connect to one another as a result of hydrodynamic effects such as convective flow, resulting in the formation of 2D-LIPSS. Based on this proposed mechanism, we have tailored the GHz burst pulses to generate intra-pulses having negatively sloped energy distributions that generate much more defined 2D-LIPSS. The results obtained to date confirm that GHz burst mode fs laser pulses can exhibit unique ablation characteristics (Kerse et al., 2016; Mishchik et al., 2019; Bonamis et al., 2020; Obata et al., 2021; Caballero-Lucas et al., 2022; Obata et al., 2023) and also have applications in micro- and nanostructuring.

The exact 2D-LIPSS formation mechanism and the geometry of such structures as created by the GHz burst mode, which may also depend on the properties of the material being processed, remain unclear. Hence, the detailed characterization of textured surfaces will be required to explore potential applications. In the present study, LIPSS were produced from titanium (Ti) substrates using GHz burst mode fs laser pulses. Ti was selected because this metal has very different physical properties from Si, which is a semiconductor. Another reason is that Ti is widely used for various industrial applications, including aircraft parts and medical implants, due to its excellent material properties such as strength, lightness, corrosion resistance and biocompatibility. Some studies have demonstrated that Ti surfaces textured to produce 1D-LIPSS using conventional irradiation techniques with fs lasers (single-pulse mode) promote cell adhesion (Oya et al., 2012; Shinonaga et al., 2015; Shinonaga et al., 2016) based on increased affinity for and compatibility with certain cells. This effect is, in turn, dependent on surface topography. Therefore, an assessment of LIPSS formation on Ti using the GHz burst mode method is important as a means of better understanding the associated formation mechanism and exploring potential applications, particularly for applications in medical implants.

2 Materials and methods

The present experiments were conducted with Ti plates polished on one side and each having a size of 10×10 mm^2 and a thickness of 1 mm. The processing was performed using linearly polarized fs laser pulses. The high-power fs Yb:KGW laser system employed in this work (Pharos, Light Conversion Ltd.) could be operated in the GHz burst mode to generate a series of fs laser pulse trains. Figure 1 presents a diagram showing the waveforms associated with the conventional single-pulse mode (Figure 1A) and the GHz burst mode (Figure 1B). Herein, a packet of fs laser pulses in a train is referred to as a burst pulse while the fs laser pulses in the burst pulse are termed intra-pulses. The numbers of burst pulses is given the symbol N while the number of intra-pulses is P. The duration and the central wavelength (λ) of the linearly polarized fs pulses were 230 fs and 1,030 nm, respectively. The repetition rate was set at 10 kHz and the time interval between each intra-pulse was 205 ps, corresponding to a repetition rate of 4.88 GHz. The shape of the burst pulse, meaning the energy distribution of the intra-pulses in the burst pulse, was controlled.

The P-value associated with each burst pulse was varied between 1 (equivalent to the single-pulse mode) and 9 to investigate the effect

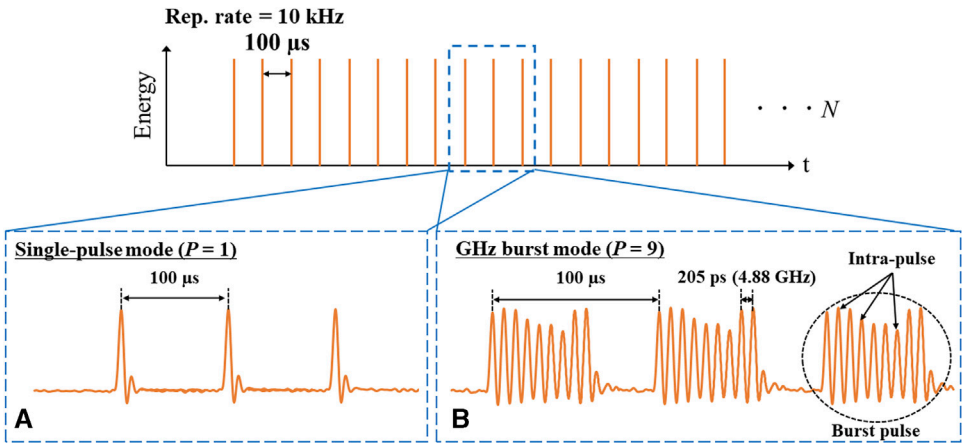

FIGURE 1
Diagrams showing fs laser pulses associated with different irradiation schemes, comprising **(A)** conventional single-pulse mode (P = 1) and **(B)** GHz burst mode with each burst consisting of nine intra-pulses (P = 9).

of this parameter on the LIPSS morphology formed on the Ti surface. Supplementary Figure S1 presents a diagram showing the experimental setup used to create LIPSS using GHz burst mode fs laser pulses. In this system, a p-polarized laser beam was applied to a Ti substrate placed on an XYZ-stage after being focused through an achromatic lens with a focal length of 50 mm. During this process, the stage was moved at a constant speed of 5 mm/s. The laser power was adjusted using polarizing optical elements, including a half-wave plate and a polarizing cubic beam splitter (PBS). The burst pulse conditions were monitored using an ultrafast photodiode connected to an oscilloscope. Specifically, a s-polarized laser beam was split using a PBS and then sent to the photodiode. The LIPSS fabricated on Ti surfaces in this manner were subsequently examined by scanning electron microscopy (SEM; Quattro S, Thermo Fisher Scientific K.K.).

The Gaussian spatial distribution of the laser fluence, $F(r)$, can be written as

$$F(r) = F_0 \exp\left(-2\frac{r^2}{w_0^2}\right), \tag{1}$$

where F_0 is the fluence at the center of the Gaussian beam, also termed the peak fluence, r is the distance from the center of the Gaussian beam and w_0 is the focal spot radius, corresponding to the position at which F_0 decreases to $1/e^2$. The laser pulse energy, E_{pulse}, is defined as

$$E_{pulse} = \int_0^{2\pi}\int_0^{\infty} F(r)dr \cdot rd\theta = \frac{F_0 \pi w_0^2}{2}, \tag{2}$$

where

$$F_0 = \frac{2E_{pulse}}{\pi w_0^2}. \tag{3}$$

Fitting the experimental data comprising the diameter of each ablated region, D, and the peak fluence, F_0, allowed both w_0 and the ablation threshold fluence, $F_{th}(n)$, for a given number of pulses, n, to be determined according to the relationship (Liu, 1982; Zemaitis et al., 2018)

$$D^2 = 2w_0^2 ln\left(\frac{F_0}{F_{th}(n)}\right). \tag{4}$$

Ti surfaces were ablated by irradiation using single-pulse mode (P = 1) with the laser beam focused at a specific position and using n values of 1, 50 and 100. Using Eq 4, w_0 was estimated to be 10.21 µm and the threshold pulse energy for each n, $E_{th}(n)$, was determined to be 249 nJ for n = 1, 134 nJ for n = 50 and 124 nJ for n = 100. The corresponding ablation threshold fluences $F_{th}(1)$, $F_{th}(50)$ and $F_{th}(100)$ were estimated to be 152, 82 and 76 mJ/cm^2, respectively.

3 Results and discussion

3.1 Effect of number of intra-pulses on LIPSS morphology

Figures 2(a2–e2), (a3–e3); Figures 2(a4–e4) present SEM images showing the Ti surface morphology produced by the GHz burst mode fs laser pulses with P-values of 1, 3, 5, 7 and 9 at average laser powers of 8, 16 and 20 mW. These values correspond to peak burst pulse fluences, F_{bp}, of 0.49, 0.98 and 1.22 J/cm^2, respectively. Note that, in these experiments, the intensity of the intra-pulses in the burst pulse was essentially constant for all F_{bp}, as indicated in Figures 2(a1–e1).

It is evident from Figures 2(a2–a4) that the single-pulse-mode fs laser pulses (P = 1) created 1D-LIPSS having periodicities of 730–840 nm (equivalent to 0.71–0.82λ). These structures were formed perpendicular to the laser polarization direction for all F_{bp}, in agreement with results previously reported by many groups (Okamuro et al., 2010; Bonse et al., 2012; Oya et al., 2012; Nathala et al., 2015; Shinonaga et al., 2015; Shinonaga et al., 2016). The GHz burst mode with P = 3 also formed 1D-LIPSS Figures 2(b2–b3) but with less nanoparticle deposition on the ridges compared with the single-pulse mode. The periods of the structures obtained using F_{bp} values of 0.49, 0.98 and 1.22 J/cm^2 were determined to be approximately 810–920 nm (0.79–0.89λ), 810–970 nm (0.79–0.94λ) and 860–1,010 nm (0.78–0.98λ), respectively.

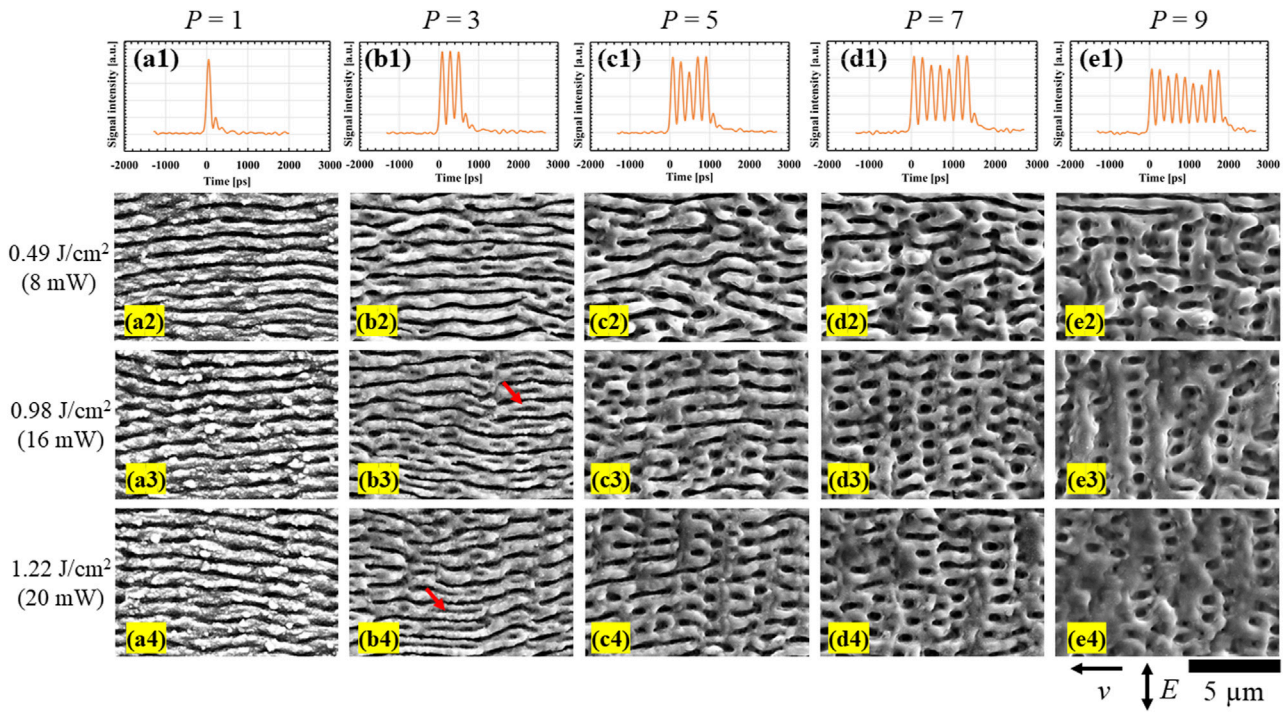

FIGURE 2
(a1–e1) Waveforms of GHz burst pulses for *P* from 1 to 9. SEM images of LIPSS formed on Ti surfaces by scanning with fs laser pulses with **(a2–a4)** single-pulse mode and **(b2–b4)**, **(c2–c4)**, **(d2–d4)** and **(e2–e4)** GHz burst mode using *P*-values of 3, 5, 7 and 9 at a constant speed of 5 mm/s, respectively. The *v* and *E* in the lower right corner indicate the directions of laser beam scanning and polarization, respectively. The pulse-to-pulse interval of intra-pulses in the burst pulse was kept constant at 205 ps. The peak laser fluence (average laser power) of the burst pulse, F_{bp}, for **(a2–e2)**, **(a3–e3)** and **(a4–e4)** was 0.49 J/cm^2 (8 mW), 0.98 J/cm^2 (16 mW) and 1.22 J/cm^2 (20 mW), respectively. The *v* and *E* in the lower right corner indicate the directions of laser beam scanning and polarization, respectively. The polarization direction is perpendicular to the scanning direction, which goes from right to left in the images.

Prior studies indicated that the period of 1D-LIPSS fabricated on Ti using single-pulse mode fs laser pulses becomes smaller as the number of pulses increases (Bonse et al., 2012; Nathala et al., 2015; Shinonaga et al., 2016). The period has also found to decrease with decreasing laser fluence (Okamuro et al., 2010; Bonse et al., 2012; Nathala et al., 2015). These experimental observations are in good agreement with a theoretical model proposed by *Sakabe et al.* (Sakabe et al., 2009) and are also supported by experimental work by *Okamuro et al.* (Okamuro et al., 2010). In contrast, in the present study, although the total number of intra-pulses was three times the number applied in single-pulse mode and the laser peak fluence for each intra-pulse, F_{ip}, was one-third that associated with single-pulse mode, the period of 1D-LIPSS formed by the GHz burst mode was larger than that generated using single-pulse mode. This discrepancy suggests that the period of 1D-LIPSS fabricated by the GHz burst mode process may be significantly affected by unique phenomena resulting from consecutive exposure to multiple pulses with an extremely high repetition rate. These phenomena may include transient changes in physical properties, such as the absorption coefficient and permittivity, due to heat accumulation. These changes could be maintained during subsequent intra-pulse irradiation and, in turn, affect the wavelength of the surface plasma wave to increase the period (Sakabe et al., 2009; Okamuro et al., 2010). Interestingly, some central parts of the ridges of the present 1D-LIPSS were found to have been ablated to produce shorter periods of 430–500 nm (0.42–0.49λ) at F_{bp} values of both 0.98 and 1.22 J/cm^2 (as indicated by the red arrows in Figures 2(b3, b4). This effect has not yet been reported and may also be related to transient changes in physical properties. The ongoing intra-pulse irradiation of 1D-LIPSS following transient variations in properties could generate SPPs having shorter wavelengths. These SPPs could be responsible for creating LIPSS exhibiting shorter periods (Bonse and Krüger, 2010; Miyaji et al., 2012; Miyazaki and Miyaji, 2013; Tjy et al., 2014; Iida et al., 2021), although further investigation is necessary.

It should also be noted that, in the case of *P*-values of 5 or greater [see Figures 2(c2–e2), (c3–e3); Figures 2(c4–e4)], the application of GHz burst mode fs laser pulses created 2D-LIPSS consisting of periodic structures both perpendicular and parallel to the laser polarization direction. This outcome was similar to the results of prior work with Si substrates by our group (Kawabata et al., 2023). Observations also showed that the period perpendicular to the laser polarization direction was smaller than that in the parallel direction for all conditions. As an example, the periods perpendicular and parallel to the laser polarization direction for $P = 7$ and $F_{bp} = 0.98$ J/cm^2 Figure 2(d3) were found to be approximately 840–970 nm (0.82–0.94λ) and 1,510–1840 nm (1.47–1.79λ), respectively. Additionally, melting and resolidification of the processed area became more prominent as *P* was increased, producing smoother surfaces on the ridges. These melting and resolidification processes likely resulted from the accumulation of excess heat as a consequence of the GHz repetition rate of the intra-pulses. The

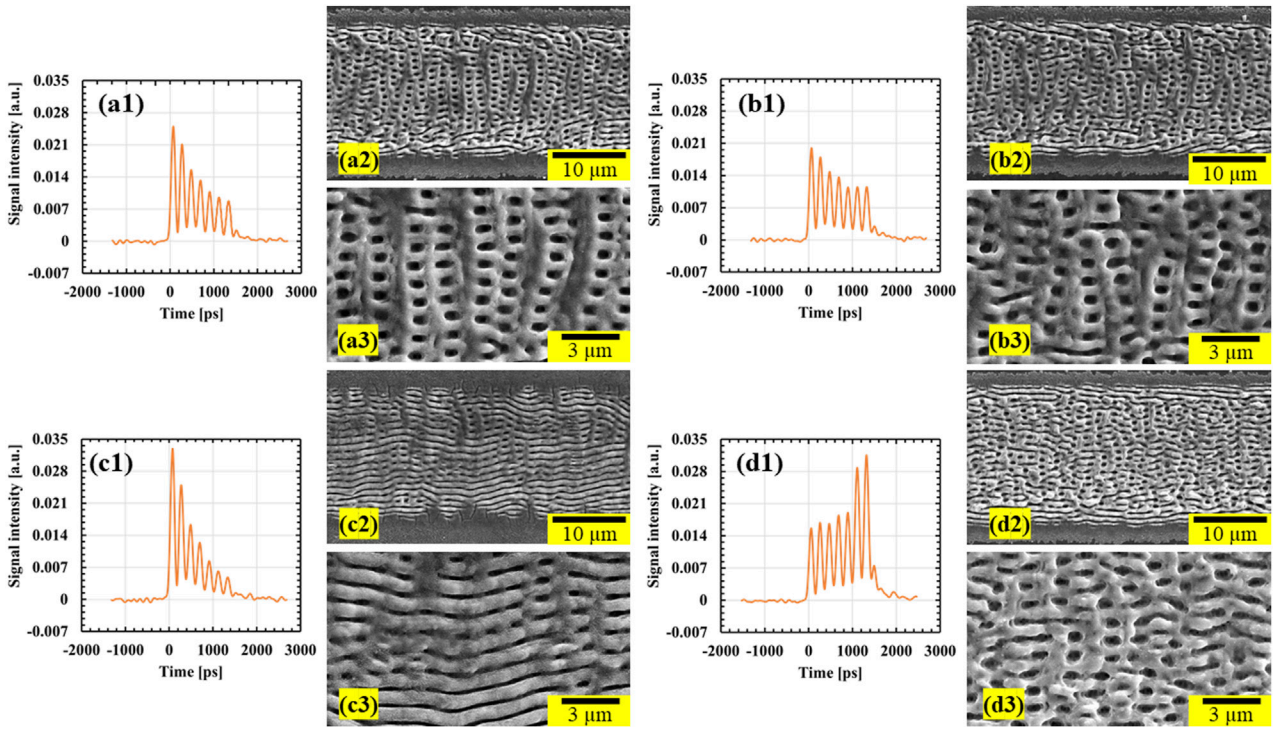

FIGURE 3
(a1–d1) Waveforms of tailored GHz burst pulses having different energy distributions for P = 7. **(a2–d2)** SEM images showing morphologies fabricated on Ti surfaces using tailored GHz burst pulses with P = 7 with F_{bp} of 0.98 J/cm^2 (16 mW) and scanning speed of 5 mm/s for energy distributions shown in **(a1–d1)**, respectively. **(a3–d3)** High-magnification versions of images in **(a2–d2)**, respectively.

minimum P-values necessary for the creation of 2D-LIPSS on Si and Ti substrates were evidently 3 and 5, respectively. This difference may be related to the different physical characteristics of these elements, such as their optical properties, photon absorption processes and electron-phonon coupling times. Nevertheless, the appearance of 2D-LIPPS on Ti in a manner similar to the results obtained with Si suggests that hot spots may have been induced by the GHz burst pulses. Nanostructured Ag and Au are known to generate hot spots associated with greatly enhanced electric fields due to the LSPR effect (Anker et al., 2008). In addition, *Jung* and *Choi* confirmed experimentally that the intensity of peaks in the Raman spectra of Ti nanodots with native oxide layers was enhanced, presumably due to the stronger electric field of the incident laser beam, although the degree of enhancement was much smaller than that observed in the case of Au (Jung and Choi, 2021). In the nanogrooves with finite length, the hot spots are a type of standing wave that occurs during the resonance, and are therefore generated periodically. Periodical generation of hot spots in the nanogrooves, which should be responsible for formation of 2D-LIPSS, has been also confirmed by finite-difference time-domain simulations (Bai et al., 2018; Kawabata et al., 2023). The geometry of 1D-LIPSS, such as the depth and width of the nanogroove created by preceding intra-pulses in a burst, is an important factor to determine the periodicity of hot spots. For further discussion of formation mechanism of 2D-LIPSS, detailed measurements of the geometry will be our future work. Another important factor is the permittivity of Ti surface. As described above, transient changes in the physical properties of the substrate including the permittivity could contribute to the generation of hot spots. We consider that the former part of intra-pulses cannot contribute to generation of the hot spots, because 2D-LIPSS cannot be created when P = 3 Figures 2(b2–b4). Meanwhile, the transient changes could be maintained during irradiation of the latter part of intra-pulse irradiation to generate the hot spots. To assess this possibility and discuss the formation mechanism of 2D-LIPSS, the periodic enhancement of electric fields associated with 1D-LIPSS on Ti will be examined by our group in the future using simulations combined with further experiments including measurement of the 1D-LIPSS geometry and identification of the permittivity change during GHz burst pulse irradiation. The melting and resolidification exhibited by the 2D-LIPSS produced in this work suggest that hydrodynamic effects contributed to the formation of these structures, which should also be investigated. Although the physical properties of Ti are significantly different from those of Si, the GHz burst mode method was also able to form 2D-LIPSS on the former metal, providing helpful insights into the 2D-LIPSS formation mechanism.

In the present study, a laser beam was scanned over the Ti surface to fabricate 2D-LIPSS having relatively large areas. As such, essentially homogeneous structures were created over the entire laser-irradiated region. This large-area texturing is critical for allowing the characterization necessary to identify practical applications for LIPSS. In the future, our group will carry out additional characterizations of these structures, such as by assessing cell growth behavior and wettability.

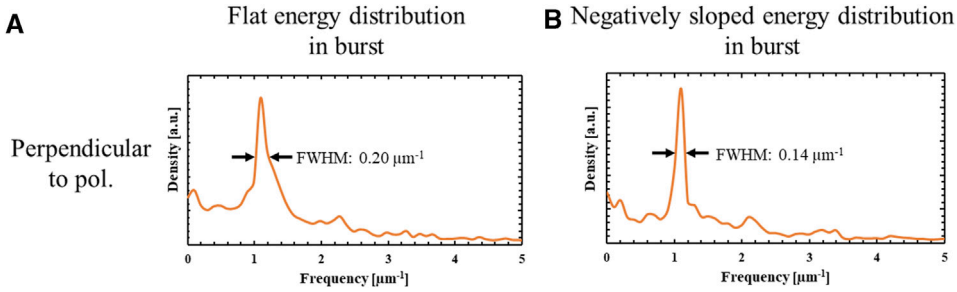

FIGURE 4
(A, B) Spatial frequency distributions analyzed by 2D Fourier transformation using the SEM images of 2D-LIPSS formed by the flat distribution (Figure 2d1) and the appropriate energy distribution with negative slope (Figure 3a1) with P = 7 and F_{bp} = 0.98 J/cm^2 (16 mW) at a scanning speed of 5 mm/s, respectively. The direction of analysis is perpendicular to the polarization direction.

3.2 Tailoring GHz burst pulses to create more well-defined 2D-LIPSS

Assuming a formation mechanism based on hot spots, the present work attempted to create more well-defined 2D-LIPSS by tuning the energy distribution of the intra-pulses in each burst pulse. It was expected that the resulting structures would be degraded by melting and resolidification as a result of overly strong electric fields generated at hot spots. To optimize this process, the envelope of the burst pulse was tailored to give a negatively sloped energy distribution. In these experiments, P and F_{bp} were fixed at 7 and 0.98 J/cm^2, respectively, and three different envelope shapes having negatively sloped distributions were employed Figures 3(a1, b1, c1). For comparison purposes, a positively sloped distribution was also employed Figure 3(d1). SEM images of the LIPSS obtained from these trials are presented in Figures 3(a2–d2) while enlarged images are shown in Figures 3(a3–d3). The morphologies of these specimens were found to be significantly affected by the distribution of the burst pulse. If the formation mechanism of 2D-LIPSS based on hot spots, which was proposed for Si, is effective for Ti, degree of the enhancement of electric field at the hot spots should be an important factor to determine the final shape of 2D-LIPSS (Kawabata et al., 2023). Since the electric field enhancement is induced by the latter part of intra-pulses, the energy distribution in the burst pulse influences the degree of enhancement. If the enhancement is too strong by relatively high energy of the latter part of intra-pulses, melting occurs at the hot spots and the resultant structure is deteriorated due to the hydrodynamic effects. In contrast, if it is too weak by relatively low energy of the latter part of intra-pulses, the electric field is insufficient to induce ablation for creation of 2D-LIPSS. Specifically, a lower negative slope value [see Figure 3(b1)] gave a 2D-LIPSS morphology Figures 3(b2, b3) that was very similar to that obtained using a flat distribution Figure 2(d3). These results are ascribed to the relatively high energy contained in the latter part of the intra-pulses, which was still able to greatly increase the electric field. In contrast, an overly high slope Figure 3(c1) did not provide 2D-LIPSS but rather generated 1D-LIPSS with a period of 900–1,000 nm (0.87–0.97λ) Figures 3(c2, c3). This morphology was similar to that obtained at P = 3 with a flat distribution shown in Figures 2(b2–b4). This change can be understood by considering that the energy contained in the latter part of the intra-pulses was insufficient to enhance the electric field. In trials in which the slope was adjusted to have a positive energy distribution, as shown in Figure 3(d1), 2D-LIPSS exhibiting significant melting and resolidification exceeding those seen in Figure 2(d3) were created (Figures 3(d2, d3)). This effect was likely due to the generation of hot spots together with greatly increased electric fields by the intense latter part of the intra-pulses. These data confirm that appropriate tuning of the burst pulses as demonstrated in Figure 3(a1) can cause melting and resolidification to be significantly suppressed, resulting in the creation of much more well-defined 2D-LIPSS Figures 3(a2, a3). The sizes of the periodic structures perpendicular and parallel to the polarization direction in this case were approximately 930–1,000 nm (0.90–0.97λ) and 1,160–1750 nm (1.13–1.70λ), respectively. To quantitatively evaluate the homogeneity of 2D-LIPSS, we analyzed spatial frequency distributions by 2D Fourier transformation using the SEM images of 2D-LIPSS formed by the flat distribution Figure 2(d1) and the appropriate energy distribution with negative slope Figure 3(a1) with P = 7 and F_{bp} = 0.98 J/cm^2 (16 mW). For more precise analysis, the wider areas of SEM images than those shown in Figure 2(d3); Figure 3(a3) were used, which are given in Supplementary Figure S2 along with information on analyzing direction. Since the periodic structures formed by the latter part of intra-pulses are parallel to the laser polarization direction, the periodicity perpendicular to the polarization direction was analyzed. Figures 4A, B present the spatial frequency spectra of periodic structures formed by the flat and negatively sloped distributions, respectively. The sharp peaks are observed around 1 μm^{-1} for both spectra. However, the full width at half maximum of 0.14 μm^{-1} for the negatively sloped distribution is significantly narrower than 0.20 μm^{-1} for the flat distribution, which quantitatively indicates that the negatively sloped GHz burst pulse can form more homogeneous 2D-LIPSS compared to the flat distribution. Therefore, these results indicate that the latter part of the intra-pulses may play an important role in determining the extent to which the electric fields at hot spots are enhanced. Furthermore, tailoring the energy distribution in the burst should be effective to reduce melting and resolidification, resulting in creating more homogeneous 2D-LIPSS. Assuming our model based on the periodic generation of hot spots, we think that 2D-LIPSS similar to those presented in this work can be formed on some

other metals and metal oxides as long as the hot spots can be generated in 1D-LIPSS. For generation of the hot spots, geometry of 1D-LIPSS and the transient physical property such as permittivity, both of which are induced by former part of intra-pulses, are important factors as discussed above. In order to make these factors fulfill the conditions for 2D-LIPSS formation, control of energy, number, and repetition rate of intra-pulses is important. In fact, the minimum *P*-value necessary for the creation of 2D-LIPSS on Ti was 5, while it is 3 for Si (Kawabata et al., 2023). Additionally, for the almost same kind of stainless steel, a high repetition rate of burst pulses (42–667 GHz) forms 1D-LIPSS (Giannuzzi et al., 2019), while a low repetition rate of burst pulses (50 MHz) can fabricate 2D-LIPSS (Wang et al., 2018). Meanwhile, it may be difficult to form 2D-LIPSS on metals with high heat conductivity such as Au, Ag, and Cu, because the irradiation of burst pulses may further cause significant melting and resolidification. Exploring the materials on which 2D-LIPSS can be formed is our future work, which will provide better insight into understanding the formation mechanism.

4 Conclusion

The formation of LIPSS on Ti substrates using GHz burst mode fs laser pulses was demonstrated. This metal has very different material properties from those of Si, which was used in prior work. The aim was to investigate the 2D-LIPSS formation mechanism in detail while controlling the geometry of these structures. We first investigated the effect of the *P*-value on the LIPSS morphology and found that using GHz burst pulses with *P*-values of 5 or higher allowed the formation of 2D-LIPSS on Ti. Based on our hypothesis regarding the formation of 2D-LIPSS, much more defined morphologies were produced by tailoring the shape of the burst pulse with an optimized *P*. Specifically, a burst pulse with $P = 7$ provided a negatively sloped energy distribution that effectively suppressed melting and resolidification to create highly defined 2D-LIPSS. However, even when employing negatively sloped distributions, an inappropriate slope magnitude did not give well-defined 2D-LIPSS. These results provide helpful insights into the 2D-LIPSS formation mechanism. Even so, further investigations are necessary, including the simulation of electric field enhancement in 1D-LIPSS and the contribution of hydrodynamic effects. Importantly, this work demonstrated that scanning with GHz burst mode fs laser pulses can create essentially homogeneous 2D-LIPSS over large areas. The unique geometries of 2D-LIPSS formed on Ti, including more complicated structures and increased surface areas, could potentially offer distinct surface functionalities that cannot be achieved with conventional 1D-LIPSS morphologies. In particular, 2D-LIPSS may have applications related to cell growth on medical implants.

Data availability statement

The original contributions presented in the study are included in the article/Supplementary Material, further inquiries can be directed to the corresponding author.

Author contributions

SK: Conceptualization, Data curation, Formal Analysis, Investigation, Methodology, Resources, Software, Visualization, Writing–original draft, Writing–review and editing. SB: Supervision, Writing–review and editing. KoO: Resources, Supervision, Writing–review and editing. KaO: Resources, Supervision, Writing–review and editing. GM: Resources, Supervision, Writing–review and editing. KS: Conceptualization, Funding acquisition, Methodology, Project administration, Resources, Supervision, Writing–original draft, Writing–review and editing.

Funding

The author(s) declare financial support was received for the research, authorship, and/or publication of this article. This study was supported by the MEXT Quantum Leap Flagship Program (MEXT Q-LEAP) through grant number JPMXS0118067246.

Acknowledgments

The authors are grateful to the Materials Characterization Support Unit at RIKEN CEMS for providing access to the SEM instrumentation used in this work. We have received support from Yasushi Minemura, Tokyo University of Agriculture and Technology, in analyzing data using the Fast Fourier Transform (FFT) method. This work was supported by RIKEN Student Researcher Program.

Conflict of interest

The authors declare that the research was conducted in the absence of any commercial or financial relationships that could be construed as a potential conflict of interest.

Publisher's note

Supplementary material

The Supplementary Material for this article can be found online at: https://www.frontiersin.org/articles/10.3389/fnano.2023.1267284/full#supplementary-material

References

Anker, J. N., Hall, W. P., Lyandres, O., Shah, N. C., Zhao, J., and Van Duyne, R. P. (2008). Biosensing with plasmonic nanosensors. *Nat. Mater* 7, 442–453. doi:10.1038/nmat2162

Bai, S., Li, Z., Obata, K., Kawabata, S., and Sugioka, K. (2023). λ/20 surface nanostructuring of ZnO by mask-less ultrafast laser processing. *Nanophotonics* 12, 1499–1510. doi:10.1515/nanoph-2022-0657

Bai, S., Serien, D., Hu, A., and Sugioka, K. (2018). 3D microfluidic surface-enhanced Raman spectroscopy (SERS) chips fabricated by all-femtosecond-laser-processing for real-time sensing of toxic substances. *Adv. Funct. Mater.* 28. doi:10.1002/adfm.201706262

Bai, S., Serien, D., Ma, Y., Obata, K., and Sugioka, K. (2020). Attomolar sensing based on liquid interface-assisted surface-enhanced Raman scattering in microfluidic chip by femtosecond laser processing. *ACS Appl. Mater Interfaces* 12, 42328–42338. doi:10.1021/acsami.0c11322

Bonamis, G., Audouard, E., Honninger, C., Lopez, J., Mishchik, K., Mottay, E., et al. (2020). Systematic study of laser ablation with GHz bursts of femtosecond pulses. *Opt. Express* 28, 27702–27714. doi:10.1364/OE.400624

Bonse, J., Höhm, S., Rosenfeld, A., and Krüger, J. (2012). Sub-100-nm laser-induced periodic surface structures upon irradiation of titanium by Ti:sapphire femtosecond laser pulses in air. *Appl. Phys. A* 110, 547–551. doi:10.1007/s00339-012-7140-y

Bonse, J., Koter, R., Hartelt, M., Spaltmann, D., Pentzien, S., Hohm, S., et al. (2014). Femtosecond laser-induced periodic surface structures on steel and titanium alloy for tribological applications. *Appl. Phys. A-Materials Sci. Process.* 117, 103–110. doi:10.1007/s00339-014-8229-2

Bonse, J., and Krüger, J. (2010). Pulse number dependence of laser-induced periodic surface structures for femtosecond laser irradiation of silicon. *J. Appl. Phys.* 108, 034903. doi:10.1063/1.3456501

Borowiec, A., and Haugen, H. K. (2003). Subwavelength ripple formation on the surfaces of compound semiconductors irradiated with femtosecond laser pulses. *Appl. Phys. Lett.* 82, 4462–4464. doi:10.1063/1.1586457

Buividas, R., Rosa, L., Sliupas, R., Kudrius, T., Slekys, G., Datsyuk, V., et al. (2011). Mechanism of fine ripple formation on surfaces of (semi)transparent materials via a half-wavelength cavity feedback. *Nanotechnology* 22, 055304. doi:10.1088/0957-4484/22/5/055304

Caballero-Lucas, F., Obata, K., and Sugioka, K. (2022). Enhanced ablation efficiency for silicon by femtosecond laser microprocessing with GHz bursts in MHz bursts(BiBurst). *Int. J. Extreme Manuf.* 4, 015103. doi:10.1088/2631-7990/ac466e

Dufft, D., Rosenfeld, A., Das, S. K., Grunwald, R., and Bonse, J. (2009). Femtosecond laser-induced periodic surface structures revisited: a comparative study on ZnO. *J. Appl. Phys.* 105, 034908. doi:10.1063/1.3074106

Edakubo, M., Richter, L. J., Haraguchi, Y., Aruga-katori, H., Ihlemann, J., and Miyaji, G. (2022). Improvement of the optical transmittance of a SiO2 surface by a femtosecond-laser-induced homogeneous nanostructure formation. *Opt. Mater. Express* 12, 3982–3989. doi:10.1364/Ome.470510

Giannuzzi, G., Gaudiuso, C., Franco, C. D., Scamarcio, G., Lugarà, P. M., and Ancona, A. (2019). Large area laser-induced periodic surface structures on steel by bursts of femtosecond pulses with picosecond delays. *Opt. Lasers Eng.* 114, 15–21. doi:10.1016/j.optlaseng.2018.10.006

Gurevich, E. L. (2016). Mechanisms of femtosecond LIPSS formation induced by periodic surface temperature modulation. *Appl. Surf. Sci.* 374, 56–60. doi:10.1016/j.apsusc.2015.09.091

Huang, M., Zhao, F., Cheng, Y., Xu, N., and Xu, Z. (2009). Origin of laser-induced near-subwavelength ripples: interference between surface plasmons and incident laser. *ACS Nano* 3, 4062–4070. doi:10.1021/nn900654v

Iida, Y., Nikaido, S., and Miyaji, G. (2021). Sub-100-nm periodic nanostructure formation induced by short-range surface plasmon polaritons excited with few-cycle laser pulses. *J. Appl. Phys.* 130, 183102. doi:10.1063/5.0069301

Jung, M., and Choi, Y.-W. (2021). Effects of native oxidation on Ti/TiO2 nanodot arrays and their plasmonic properties compared to Au nanodot arrays. *Appl. Surf. Sci.* 554, 149636. doi:10.1016/j.apsusc.2021.149636

Kawabata, S., Bai, S., Obata, K., Miyaji, G., and Sugioka, K. (2023). Two-dimensional laser-induced periodic surface structures formed on crystalline silicon by GHz burst mode femtosecond laser pulses. *Int. J. Extreme Manuf.* 5, 015004. doi:10.1088/2631-7990/acb133

Kerse, C., Kalaycioglu, H., Elahi, P., Cetin, B., Kesim, D. K., Akcaalan, O., et al. (2016). Ablation-cooled material removal with ultrafast bursts of pulses. *Nature* 537, 84–88. doi:10.1038/nature18619

Levy, Y., Derrien, T. J. Y., Bulgakova, N. M., Gurevich, E. L., and Mocek, T. (2016). Relaxation dynamics of femtosecond-laser-induced temperature modulation on the surfaces of metals and semiconductors. *Appl. Surf. Sci.* 374, 157–164. doi:10.1016/j.apsusc.2015.10.159

Liu, J. M. (1982). Simple technique for measurements of pulsed Gaussian-beam spot sizes. *Opt. Lett.* 7, 196–198. doi:10.1364/ol.7.000196

Mishchik, K., Bonamis, G., Qiao, J., Lopez, J., Audouard, E., Mottay, E., et al. (2019). High-efficiency femtosecond ablation of silicon with GHz repetition rate laser source. *Opt. Lett.* 44, 2193–2196. doi:10.1364/OL.44.002193

Miyaji, G., Miyazaki, K., Zhang, K., Yoshifuji, T., and Fujita, J. (2012). Mechanism of femtosecond-laser-induced periodic nanostructure formation on crystalline silicon surface immersed in water. *Opt. Express* 20, 14848–14856. doi:10.1364/OE.20.014848

Miyazaki, K., and Miyaji, G. (2013). Nanograting formation through surface plasmon fields induced by femtosecond laser pulses. *J. Appl. Phys.* 114, 153108. doi:10.1063/1.4826078

Nathala, C. S., Ajami, A., Ionin, A. A., Kudryashov, S. I., Makarov, S. V., Ganz, T., et al. (2015). Experimental study of fs-laser induced sub-100-nm periodic surface structures on titanium. *Opt. Express* 23, 5915–5929. doi:10.1364/OE.23.005915

Obata, K., Caballero-Lucas, F., Kawabata, S., Miyaji, G., and Sugioka, K. (2023). GHz bursts in MHz burst (BiBurst) enabling high-speed femtosecond laser ablation of silicon due to prevention of air ionization. *Int. J. Extreme Manuf.* 5, 025002. doi:10.1088/2631-7990/acc0e5

Obata, K., Caballero-Lucas, F., and Sugioka, K. (2021). Material processing at GHz burst mode by femtosecond laser ablation. *J. Laser Micro/Nanoeng* 16, 19–23. doi:10.2961/jlmn.2021.01.2004

Okamuro, K., Hashida, M., Miyasaka, Y., Ikuta, Y., Tokita, S., and Sakabe, S. (2010). Laser fluence dependence of periodic grating structures formed on metal surfaces under femtosecond laser pulse irradiation. *Phys. Rev. B* 82, 165417. doi:10.1103/PhysRevB.82.165417

Oya, K., Aoki, S., Shimomura, K., Sugita, N., Suzuki, K., Nakamura, N., et al. (2012). Morphological observations of mesenchymal stem cell adhesion to a nanoperiodic-structured titanium surface patterned using femtosecond laser processing. *Jpn. J. Appl. Phys.* 51, 125203. doi:10.1143/jjap.51.125203

Reif, J., Varlamova, O., and Costache, F. (2008). Femtosecond laser induced nanostructure formation: self-organization control parameters. *Appl. Phys. A* 92, 1019–1024. doi:10.1007/s00339-008-4671-3

Sakabe, S., Hashida, M., Tokita, S., Namba, S., and Okamuro, K. (2009). Mechanism for self-formation of periodic grating structures on a metal surface by a femtosecond laser pulse. *Phys. Rev. B* 79, 033409. doi:10.1103/PhysRevB.79.033409

Sato, Y., Tsukamoto, M., Shinonaga, T., and Kawa, T. (2016). Femtosecond laser-induced periodic nanostructure creation on PET surface for controlling of cell spreading. *Appl. Phys. A* 122, 184. doi:10.1007/s00339-016-9716-4

Shimotsuma, Y., Kazansky, P. G., Qiu, J., and Hirao, K. (2003). Self-organized nanogratings in glass irradiated by ultrashort light pulses. *Phys. Rev. Lett.* 91, 247405. doi:10.1103/PhysRevLett.91.247405

Shinonaga, T., Kinoshita, S., Okamoto, Y., Tsukamoto, M., and Okada, A. (2016). Formation of periodic nanostructures with femtosecond laser for creation of new functional biomaterials. *Procedia CIRP* 42, 57–61. doi:10.1016/j.procir.2016.02.188

Shinonaga, T., Tsukamoto, M., Kawa, T., Chen, P., Nagai, A., and Hanawa, T. (2015). Formation of periodic nanostructures using a femtosecond laser to control cell spreading on titanium. *Appl. Phys. B-Lasers Opt.* 119, 493–496. doi:10.1007/s00340-015-6082-4

Tamamura, Y., and Miyaji, G. (2019). Structural coloration of a stainless steel surface with homogeneous nanograting formed by femtosecond laser ablation. *Opt. Mater. Express* 9, 2902–2909. doi:10.1364/Ome.9.002902

Tjy, D., Koter, R., Krüger, J., Höhm, S., Rosenfeld, A., and Bonse, J. (2014). Plasmonic formation mechanism of periodic 100-nm-structures upon femtosecond laser irradiation of silicon in water. *J. Appl. Phys.* 116, 074902. doi:10.1063/1.4887808

Tsukamoto, M., Asuka, K., Nakano, H., Hashida, M., Katto, M., Abe, N., et al. (2006). Periodic microstructures produced by femtosecond laser irradiation on titanium plate. *Vacuum* 80, 1346–1350. doi:10.1016/j.vacuum.2006.01.016

Varlamova, O., Costache, F., Reif, J., and Bestehorn, M. (2006). Self-organized pattern formation upon femtosecond laser ablation by circularly polarized light. *Appl. Surf. Sci.* 252, 4702–4706. doi:10.1016/j.apsusc.2005.08.120

Vorobyev, A. Y., and Guoa, C. L. (2008). Colorizing metals with femtosecond laser pulses. *Appl. Phys. Lett.* 92, 041914. doi:10.1063/1.2834902

Wagner, R., and Gottmann, J. (2007). Sub-wavelength ripple formation on various materials induced by tightly focused femtosecond laser radiation. *J. Phys. Conf. Ser.* 59, 333–337. doi:10.1088/1742-6596/59/1/070

Wang, X., Li, C., Ma, C., Feng, J., Hong, W., and Zhang, Z. (2018). Formation of laser induced periodic structures on stainless steel using multi-burst picosecond pulses. *Opt. Express* 26, 6325–6330. doi:10.1364/OE.26.006325

Zemaitis, A., Gaidys, M., Brikas, M., Gecys, P., Raciukaitis, G., and Gedvilas, M. (2018). Advanced laser scanning for highly-efficient ablation and ultrafast surface structuring: experiment and model. *Sci. Rep.* 8, 17376. doi:10.1038/s41598-018-35604-z